



Characterization of neoantigen-specific T cells in cancer resistant to immune checkpoint therapies

Shamin Li^{a,1}, Yannick Simon^{a,b}, Summer Zhuang^a, Austin Gabel^{c,d,e,f}, Shaokang Ma^g, Jonathan Chee^g, Laura Islas^a, Anthony Cessna^a, Jenette Creaney^{g,h,i}, Robert K. Bradley^{c,d,e}, Alec Redwood^g, Bruce W. Robinson^g, and Evan W. Newell^{a,1}

^aVaccine and Infectious Diseases Division, Fred Hutchinson Cancer Research Center, Seattle, WA 98109; ^bImmunoSCAPE, Pte Ltd, Singapore, 228208 Singapore; ^cComputational Biology Program, Public Health Sciences Division, Fred Hutchinson Cancer Research Center, Seattle, WA 98109; ^dBasic Sciences Division, Fred Hutchinson Cancer Research Center, Seattle, WA 98109; ^eDepartment of Genome Sciences, University of Washington, Seattle, WA 98195; ^fMedical Scientist Training Program, University of Washington, Seattle, WA 98195; ^gNational Centre for Asbestos Related Disease, Faculty of Health and Medical Science, University of Western Australia, 6009 Perth, Australia; ^hDepartment of Respiratory Medicine, Sir Charles Gairdner Hospital, 6009 Perth, Australia; and ⁱInstitute for Respiratory Health, University of Western Australia, 6009 Perth, Australia

Edited by Rafi Ahmed, Emory University, Atlanta, GA, and approved June 16, 2021 (received for review December 14, 2020)

Neoantigen-specific T cells are strongly implicated as being critical for effective immune checkpoint blockade treatment (ICB) (e.g., anti-PD-1 and anti-CTLA-4) and are being targeted for vaccination-based therapies. However, ICB treatments show uneven responses between patients, and neoantigen vaccination efficiency has yet to be established. Here, we characterize neoantigen-specific CD8⁺ T cells in a tumor that is resistant to ICB and neoantigen vaccination. Leveraging the use of mass cytometry combined with multiplex major histocompatibility complex (MHC) class I tetramer staining, we screened and identified tumor neoantigen-specific CD8⁺ T cells in the Lewis Lung carcinoma (LLC) tumor model (mRiok1). We observed an expansion of mRiok1-specific CD8⁺ tumor-infiltrating lymphocytes (TILs) after ICB targeting PD-1 or CTLA-4 with no sign of tumor regression. The expanded neoantigen-specific CD8⁺ TILs remained phenotypically and functionally exhausted but displayed cytotoxic characteristics. When combining both ICB treatments, mRiok1-specific CD8⁺ TILs showed a stem-like phenotype and a higher capacity to produce cytokines, but tumors did not show signs of regression. Furthermore, combining both ICB treatments with neoantigen vaccination did not induce tumor regression either despite neoantigen-specific CD8⁺ TIL expansion. Overall, this work provides a model for studying neoantigens in an immunotherapy nonresponder model. We showed that a robust neoantigen-specific T-cell response in the LLC tumor model could fail in tumor response to ICB, which will have important implications in designing future immunotherapeutic strategies.

LLC | CyTOF | immunotherapies | neoantigen | vaccination

Currently, one of the most successful immunotherapeutic interventions for treating cancers is targeting T cell checkpoints such as PD-1 or CTLA-4, that improve the effector T cell response through distinct pathways (1, 2). Both inhibitors have showed promising results, improving both patient outcomes and overall survival. However, with an unpredictable and uneven response across different cancer types and treatment settings (3, 4), the efficacy of these therapies needs to be improved.

In this context, presence of neoantigens in the tumor cells—unique mutated proteins derived from either viral oncogenic proteins or nonsynonymous somatic mutations—elicits a potent immune response that improves treatment efficacy (5–11). While this is especially true in tumors with a high tumor mutational burden (TMB) and thus a high neoantigen load, recent studies showed a likely better correlation between neoantigen immunogenicity and treatment response (8, 12, 13). Although neoantigen discovery could lead to some very attractive therapeutics (including adoptive T cell therapy and neoantigen vaccine) (14–16), the challenges of predicting and identifying neoantigens remain (8, 17). In addition, since TMB is not perfectly predictive, more is to be learned about how to efficiently tackle neoantigen-associated therapies (18, 19).

In mice, neoantigens have been studied mostly in immunotherapy responder models (20–23). In d42m1-T3 methylcholanthrene

(MCA) sarcoma for instance, two immunodominant neoantigens have been identified and showed to be reactivated upon anti-PD-1 and/or anti-CTLA-4 blockade, enabling an effective tumor rejection that could be boosted via neopeptide-based vaccination (21). Notably, using mass cytometry, CD8⁺ tumor-infiltrating lymphocytes (TILs) that are specific for these neoantigens showed a dramatic phenotypic change between treated versus untreated tumors (22, 24), leading to the question as to whether the phenotypes of neoantigen-specific CD8⁺ TILs could accurately predict treatment outcome. This concept has been extensively studied in the recent years to identify reliable biomarkers for immunotherapy response, and numerous works have addressed the paradigm of “exhausted” versus “precursor exhausted” T cells (25–29). While “exhausted” T cells are often associated with dysfunction and reduced capacity to control tumor growth, “precursor exhausted” refers to T cells capable of proliferation after immunotherapy that maintain memory characteristics and a long-term effective T cell response (27). As each of these populations is well characterized with a

Significance

Strongly implicated in effective antitumor immune responses, tumor mutation-derived antigens, or neoantigens, are one of the main targets for cancer vaccines despite uncertainty of the efficacy of this approach. Using a high-throughput screening method, we identify an endogenously immunogenic neoantigen in a commonly used mouse lung tumor model. We also found that the endogenous CD8 T cells specific for this neoantigen expand greatly upon treatment with immune checkpoint inhibitors or vaccination despite the lack of associated tumor regression in this model. In addition to informing neoantigen vaccination strategies and providing an accessible system for testing alternative therapeutics, our results provide insights into the mechanisms for the lack of response observed for a majority of patients treated with checkpoint blockade immunotherapies.

Author contributions: S.L. designed research; S.L., S.Z., A.G., S.M., L.I., and A.C. performed research; E.W.N. contributed new reagents/analytic tools; S.L., Y.S., J. Chee, J. Creaney, R.K.B., A.R., and B.W.R. analyzed data; S.L. and E.W.N. wrote the paper; Y.S. discussed the data and reviewed the paper; S.Z. and A.G. reviewed the paper; J. Chee, J. Creaney, R.K.B., A.R., and B.W.R. discussed the data; and E.W.N. led the project.

Competing interest statement: E.W.N. is a cofounder, advisor, and shareholder of ImmunoScape Pte. Ltd. E.W.N. is an advisor for Neogene Therapeutics and Nanostring Technologies.

This article is a PNAS Direct Submission.

This open access article is distributed under Creative Commons Attribution-NonCommercial-NoDerivatives License 4.0 (CC BY-NC-ND).

¹To whom correspondence may be addressed. Email: enewell@fredhutch.org or shaminli@fredhutch.org.

This article contains supporting information online at <https://www.pnas.org/lookup/suppl/doi:10.1073/pnas.2025570118/-DCSupplemental>.

Published July 20, 2021.

unique protein, transcriptomic, and epigenetic signature, assessing the profile of tumor-specific CD8⁺ T cells in this setting would be important to understand their role and reshape their response in immunotherapy (30).

Here, we use a syngeneic model of lung cancer in mice widely described as nonresponsive to immune checkpoint blockade (31–34). With the advantage of being derived from a spontaneous tumor, we hypothesize that neoantigen-specific T cells in Lewis Lung carcinoma (LLC) are elicited despite a relatively low tumor mutational burden and nonresponsiveness to checkpoint blockade immunotherapy. We first validated the neoantigen prediction performed with bioinformatic approaches by *ex vivo* screening of the neopeptides using mass cytometry and further analyzed the role of tumor-specific CD8⁺ T cells in tumors resistant to immune checkpoint blockade therapy.

Results

Identification and Characterization of Neoantigen-Specific CD8⁺ T Cells in LLC. In order to screen for neoantigen-specific CD8⁺ T cells in LLC, we sequenced the transcriptome of normal and tumor tissues to identify tumor-specific mutations. *In silico*, we predicted 209 neoantigen peptides following our criteria of selection (Fig. 1A and Table S1; *Materials and Methods*). To identify CD8⁺ T cells specific for these neoantigens, we combined the use of mass cytometry with multiplex MHC class I tetramer staining strategy as previously described (22, 35, 36). Briefly, each peptide-MHC (pMHC) was tagged with a unique triple-coding streptavidin scheme, allowing for detection of 220 different tetramers in a cytometry by time-of-flight (CyTOF) panel that used 12 channels for metal-tagged streptavidins (SAV) (Fig. 1B; *Materials and Methods*). The remaining mass cytometry channels were dedicated to T cell-targeted phenotypic markers (Table S2). LLC tumors were collected from B6 mice between day 14 and 16 after tumor inoculation, processed and enriched for both CD45⁺ and T cells, and stained with the multiplex tetramer mixture followed by surface antibodies (*Materials and Methods*). Samples were acquired on the Helios mass cytometer and analyzed using dimension reduction algorithms such as Uniform Manifold Approximation and Projection (UMAP) [*Materials and Methods* (37); Fig. 1C]. Neoantigen-specific T cells were defined as CD8⁺ T cells positive for an exact three-SAV code. Among the 209 MHC class I tetramers that were simultaneously used, we detected only one tetramer hit (KMYQYARL), with a G946T mutation on the gene R10K1 that we will call mRiok1 from now on (Table S1 and Fig. 1D). As negative controls, we showed the expression of all SAV for this neoantigen, and we did not detect cells positive for this tetramer in the CD4⁺ or CD4[−] CD8[−] T cell compartment (*SI Appendix, Fig. S1 A and B*). Furthermore, we validated by flow cytometry the presence of neoantigen mRiok1-specific CD8⁺ T cells in LLC tumors (Fig. 1E), and we were as well able to detect these cells in different peripheral organs at lower frequencies (*SI Appendix, Fig. S1C*).

We next investigated the phenotype of mRiok1-specific CD8⁺ T cells in LLC tumors and peripheral organs. Based on the UMAP plot, we observed several cell clusters in the tumors that indicated a heterogeneous composition of CD8⁺ TILs (Fig. 1F and *SI Appendix, Fig. S1D*). These cell clusters showed characteristics of effector (CD69[−] CD44⁺), tissue resident memory (CD69⁺, CD44⁺, and CD103^{+/−}), or exhausted (PD-1⁺, CD39⁺) cells (Fig. 1F). When plotting mRiok1-specific CD8⁺ T cells above total CD8⁺ T cells, we observed that these cells mostly fell into the exhausted cluster, with a high expression of exhaustion markers including CD39 (51 ± 17%), Tim-3 (65 ± 12%), and PD-1 (80 ± 13%) (Fig. 1G). In the periphery, mRiok1-specific CD8⁺ T cells showed a different phenotype. With a profile similar between draining lymph nodes and spleen, mRiok1-specific CD8⁺ T cells expressed a central memory phenotype (CD27⁺ CD62L⁺ CD44⁺), whereas they expressed CD39 and are negative for CD62L in the

lungs (*SI Appendix, Fig. S1 D and E*). Our observations indicated the presence of exhausted neoantigen-specific CD8⁺ TILs that could potentially play a role in LLC antitumor response.

Neoantigen-Specific T Cells Expand in Tumors Resistant to Anti-PD-1 and -CTLA-4 Therapies. Since neoantigen mRiok1-specific CD8⁺ TILs were exhausted and expressed PD-1, we next assessed the efficacy of anti-PD-1 treatments in our experimental settings. We measured the tumor volume between day 7 and 16 in the control group (treated with isotype IgG2a) and in mice treated with anti-PD-1 antibody (Fig. 2A). We did not observe any significant difference in tumor growth between both groups, indicating that LLC tumor was resistant to anti-PD-1 therapy. Interestingly, we detected a significant expansion of mRiok1-specific CD8⁺ TILs in anti-PD-1-treated mice, reaching up to 20% of total CD8⁺ TILs (mean 11 ± 5%) and 8% of total TILs (mean 3.8 ± 2.5%) (Fig. 2B). As anti-CTLA-4 blockade has also been shown to enhance tumor-specific CD8 T cell response in cancer (38, 39), we treated LLC tumors with anti-CTLA-4 or the isotype control (IgG2b) (Fig. 2C). Similar to anti-PD-1 treatment, anti-CTLA-4 blockade did not induce any significant regression in tumor growth compared to the control group, showing that LLC tumor was also resistant to anti-CTLA-4 therapy. As observed during anti-PD-1 treatment, the frequency of mRiok1-specific CD8⁺ TILs increased in anti-CTLA-4-treated mice, reaching 8% of CD8⁺ TILs (mean 4.7 ± 2.8%) and 3% of total TILs (mean 1.4 ± 1%) (Fig. 2D).

As we wanted to explore the kinetics of this expansion, we assessed the frequency of mRiok1-specific CD8⁺ TILs at different timepoints by harvesting LLC tumors from different conditions 2 d after each treatment—at day 9, 13, and 16. We detected a continuous expansion of mRiok1-specific CD8⁺ TILs in treated mice over time compared with the control group and starting as early as the first antibody treatment (*SI Appendix, Fig. S2*). In addition, parallel evaluation of Ki-67 expression in both anti-PD-1- or anti-CTLA-4-treated mice confirmed the specific proliferation of mRiok1-tet⁺ CD8 TILs, which expansion reached the maximum at day 16 (Fig. 2E).

Taken together, these results showed that LLC tumors were resistant to anti-PD-1 or anti-CTLA-4 therapy. However, both therapies induced an expansion of neoantigen-specific T cells.

Neoantigen-Specific T Cells Remain Exhausted after Anti-PD-1 or Anti-CTLA-4 Treatment. We next investigated the phenotypic changes of mRiok1-specific CD8⁺ TILs during anti-PD-1 or anti-CTLA-4 treatment. UMAP analysis showed that mRiok1-specific CD8⁺ TILs after anti-PD-1 maintained the same phenotype as in isotype-treated mice, with a slight but not significant increase of exhaustion markers expression such as CD39 and Tim3 (Fig. 3A). CD73 expression on neoantigen-specific CD8⁺ TILs was found to be significantly lower in anti-PD-1-treated tumors, suggesting T cell exhaustion status as well (40–42). Of note, we observed a decrease of CD103 expression on neoantigen-specific CD8⁺ TILs after anti-PD-1 treatment, which is reported to be associated with a poor clinical outcome (43–45). As for anti-CTLA-4-treated tumors, neoantigen-specific CD8⁺ TILs also displayed a similar phenotype compared with the isotype group, except for ICOS, which was elevated after anti-CTLA-4 treatment (Fig. 3B). Similar to anti-PD-1-treated tumors, we observed a decrease of CD73 expression on neoantigen-specific CD8⁺ TILs after anti-CTLA-4, confirming the exhausted phenotype of these cells after both therapies.

Additionally, we investigated the functional properties of neoantigen-specific T cells after anti-PD-1 or anti-CTLA-4 treatment. We first evaluated the production of Granzyme B (GzB), a secreted molecule inducing apoptosis in tumor cells and associated with exhaustion status (27). Analysis at different treatments timepoints showed that neoantigen-specific CD8⁺ TILs accumulated as CD39⁺ GzB⁺ cells in the tumors after anti-PD-1 or anti-CTLA-4 therapy, just as in the untreated group (Fig. 3C). Next, we measured

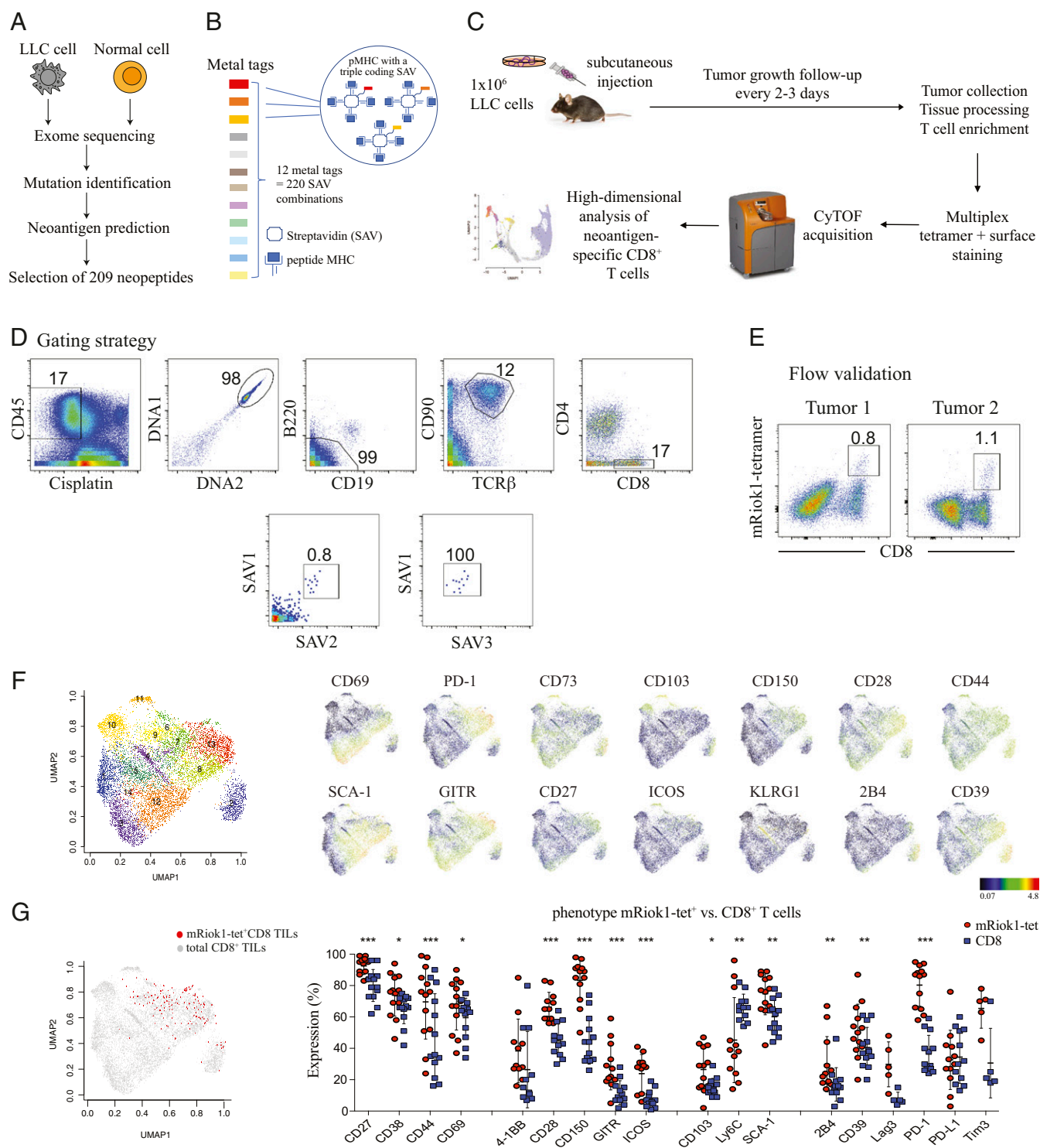


Fig. 1. Identification and characterization of neoantigen-specific CD8⁺ T cells in LLC. (A) Schematic of tumor neoantigen prediction. (B) Multiplex tetramer staining as described previously (35, 36). Each predicted H2kb neoepitope is bound to a triple-coding SAV configuration, and the use of 12 different metal-tagged SAV allows for screening of 220 different neoepitopes. (C) Experimental design for screening tumor neoantigen-specific CD8⁺ T cells in LLC by mass cytometry. (D) Mass cytometry gating strategy for tumor neoantigen-specific CD8⁺ T cells in LLC tumors. (E) Flow cytometry validation of the tetramer staining in two different LLC tumors. (F) UMAP plot of total CD8⁺ TILs in three concatenated LLC tumor samples (Left). Color plots showing expression intensities of immune markers included in the CyTOF panel (Right). (G) UMAP plot of mRiok1-tet⁺CD8⁺ TILs (red) on top of total CD8⁺ TILs (gray). Expression of different immune markers on mRiok1-tet⁺CD8⁺ TILs versus total CD8⁺ TILs. *n* = 5 to 13, means with SD; data are from at least three different experiments, paired Student's *t* test.

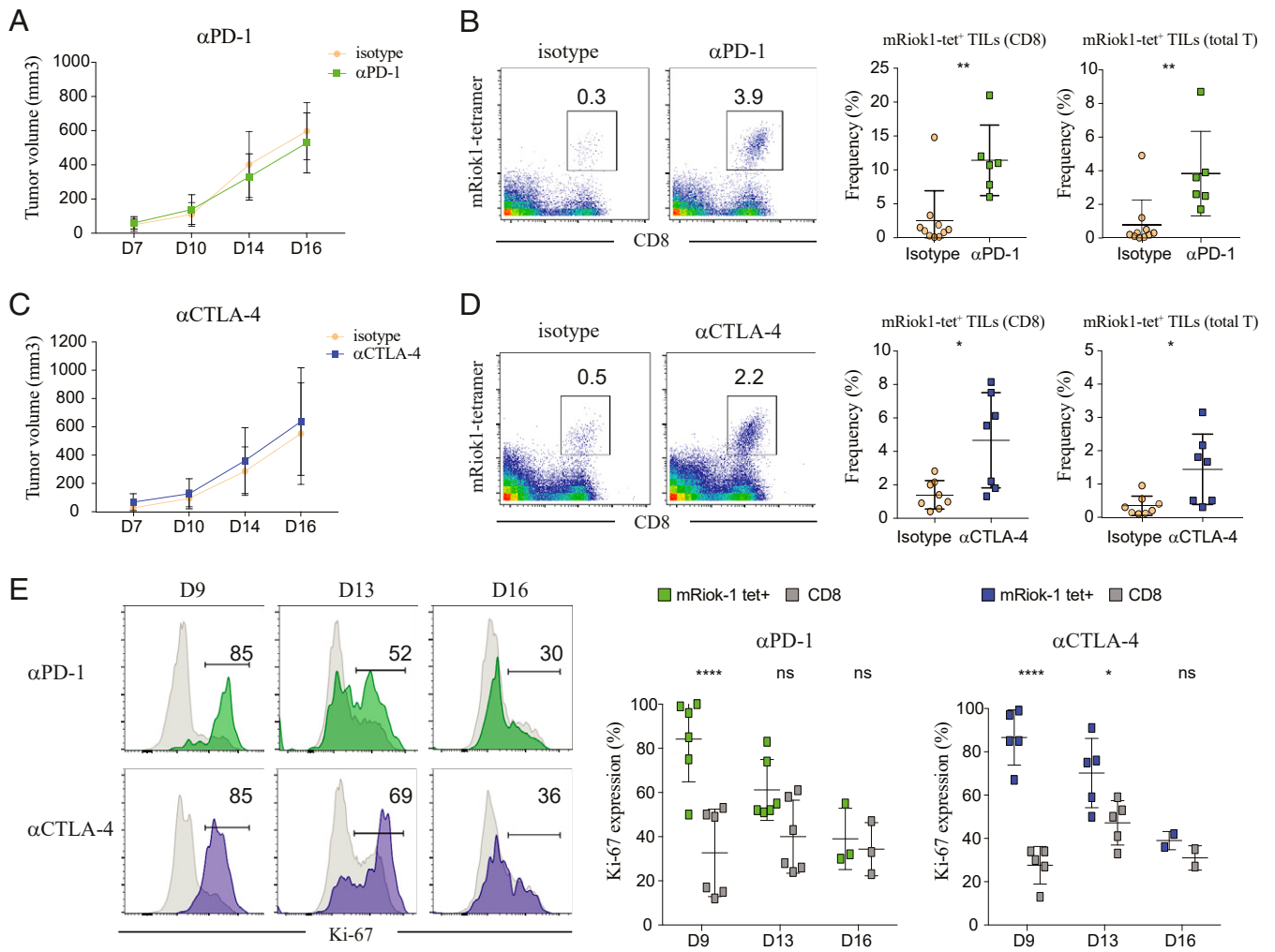


Fig. 2. Expansion of neoantigen-specific CD8⁺ T cells upon immune checkpoint blockade. (A) LLC tumor growth measured as tumor volume in mm³ ((length × width²) / 2) throughout treatment with anti-PD-1 or isotype antibody. *n* = 8 to 31, data from five independent experiments, unpaired Student's *t* tests. (B) Representative mRiok1-tetramer staining among total TILs, gated against CD8 (Left). Frequencies of mRiok1-tet⁺ TILs among total CD8⁺ TILs and total TILs (Right). *n* = 6 to 10, means with SD, data from two independent experiments, Mann-Whitney unpaired *t* test. (C) LLC tumor growth measured as tumor volume in mm³ ((length × width²) / 2) throughout treatment with anti-CTLA-4 or isotype antibody. *n* = 9 to 26, data from five independent experiments, unpaired Student's *t* tests. (D) Representative mRiok1-tetramer staining among total TILs, gated against CD8 (Left). Frequencies of mRiok1-tet⁺ TILs among total CD8⁺ TILs and total TILs (Right). *n* = 7 to 8, means with SD, data from two independent experiments, Mann-Whitney unpaired *t* test. (E) Ki-67 expression on mRiok1-tet⁺ (green for anti-PD-1 and blue for anti-CTLA-4) or total CD8⁺ TILs (gray) at different timepoints of each monotherapy. *n* = 5 to 6, means with SD, data from two independent experiments.

the production of IFN- γ and TNF- α , two cytokines implicated in antitumor responses. Following stimulation with Phorbol 12-myristate 13-acetate (PMA)/Ionomycin, we observed that neoantigen-specific CD8⁺ TILs were not capable of cytokine production and did not show any improvement after anti-PD-1 or anti-CTLA-4 treatment as compared to the isotype control (Fig. 3D).

These data provided a deep profiling of neoantigen mRiok1-specific CD8⁺ TILs upon immune checkpoint blockade and showed that the expanded mRiok1-specific CD8⁺ TILs after anti-PD-1 or anti-CTLA-4 treatment accumulated in the tumors and remained phenotypically and functionally exhausted.

Combining Anti-PD-1 and Anti-CTLA-4 Blockades Slightly Improves Tumor Response with Functional Stem-Like Neoantigen-Specific T Cells. As anti-PD-1 and anti-CTLA-4 treatment distinctively affects the tumor-infiltrating CD8 immune response, we assessed the effects of combination therapy (21, 46, 47). As compared to the control group, combined treatment with both anti-PD-1 and

anti-CTLA-4 showed an overall slower tumor growth from day 10 after tumor inoculation, despite a fairly high range of tumor volumes across experiments (Fig. 4A). Similar to monotherapy, we detected an expansion of neoantigen-specific CD8⁺ TILs after combination therapy as compared to the control group, reaching up to 40% of total CD8⁺ TILs (mean $13.3 \pm 11\%$) and 28% of total TILs (mean $5.8 \pm 8\%$) (Fig. 4B). Comprehensive CyTOF profiling revealed that neoantigen-specific CD8⁺ TILs from anti-PD-1 + anti-CTLA-4-treated mice more frequently expressed SCA-1, suggesting acquisition of a memory stem-like phenotype (Fig. 4C) (48). This was reported for neoantigen-specific CD8⁺ TILs in MCA sarcoma after effective anti-CTLA-4 treatment as well (22). mRiok1-specific CD8⁺ TILs also expressed less CD73 in anti-PD-1 + anti-CTLA-4-treated mice, as seen previously in monotherapy conditions. Interestingly, we found that neoantigen-specific CD8⁺ TILs highly expressed CD28 and ICOS, two markers associated with stem-like properties for CD8⁺ TILs (28, 49) (Fig. 4C and D). To further validate the acquisition of a stem-like phenotype for

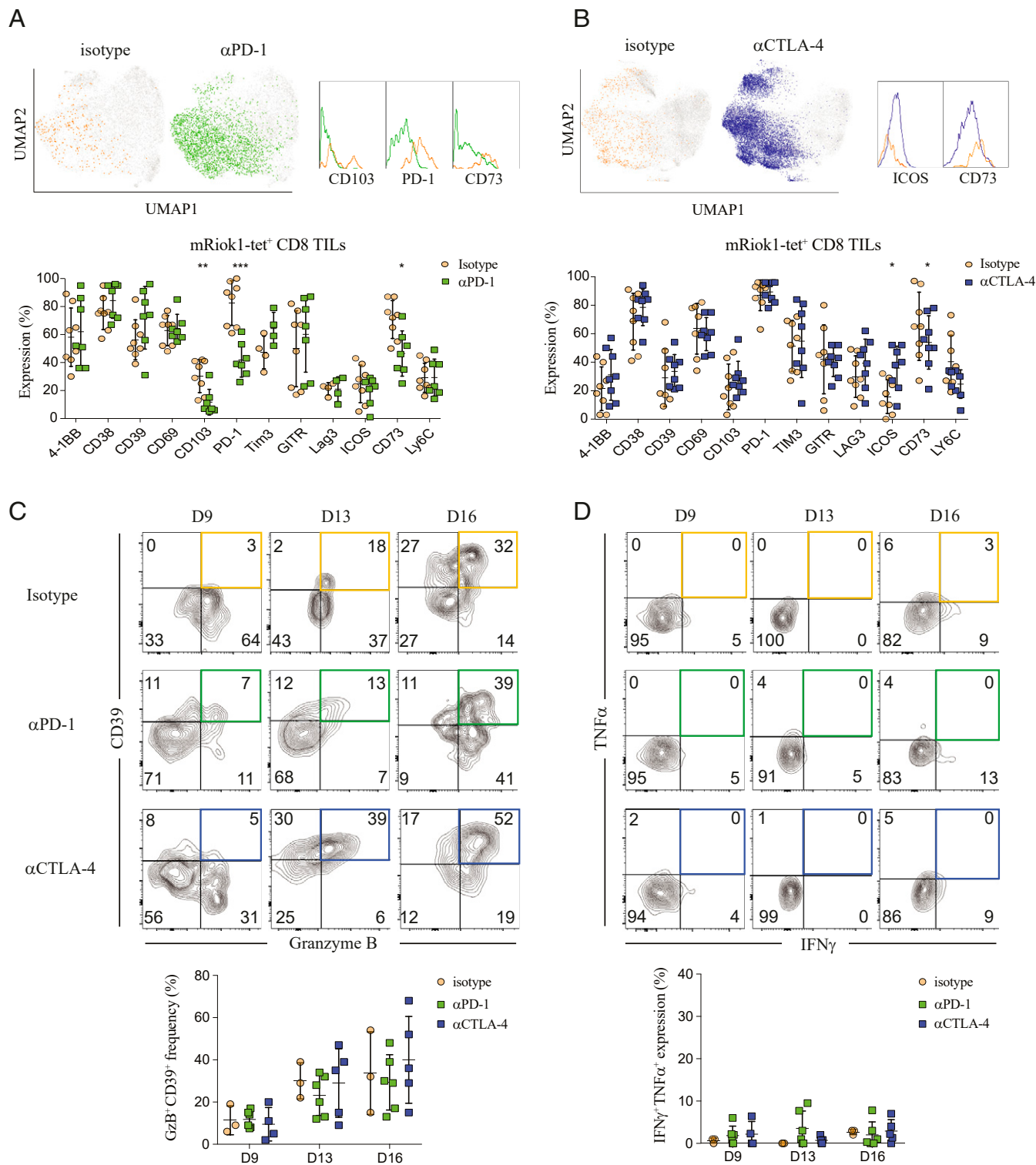


Fig. 3. Neoantigen-specific T cells remain exhausted after anti-PD-1 or anti-CTLA-4 treatment. (A) UMAP plots of mRiok1-tet⁺CD8⁺ TILs from isotype (orange) or anti-PD-1 (green)-treated tumors (Top), $n = 4$. Expression of selected markers from both conditions (Bottom), $n = 6$ to 10, means with SD, data from two independent experiments, Mann-Whitney unpaired t test. (B) UMAP plots of mRiok1-tet⁺CD8⁺ TILs from isotype (orange) or anti-CTLA-4 (blue)-treated tumors (Top), $n = 4$. Expression of selected markers from both conditions (Bottom), $n = 8$, means with SD, data from two independent experiments, Mann-Whitney unpaired t test. (C) CD39 versus Granzyme B expression on mRiok1-tet⁺CD8⁺ TILs at different timepoints of the treatments. $n = 6$ for anti-PD-1, $n = 5$ for anti-CTLA-4, and $n = 3$ for isotype control; means with SD, data from two independent experiments. (D) TNF- α and IFN- γ production on mRiok1-tet⁺CD8⁺ TILs upon PMA/Ionomycin stimulation at different timepoints of the treatments. $n = 6$ for anti-PD-1, $n = 5$ for anti-CTLA-4, and $n = 3$ for isotype control; means with SD, data from two independent experiments.

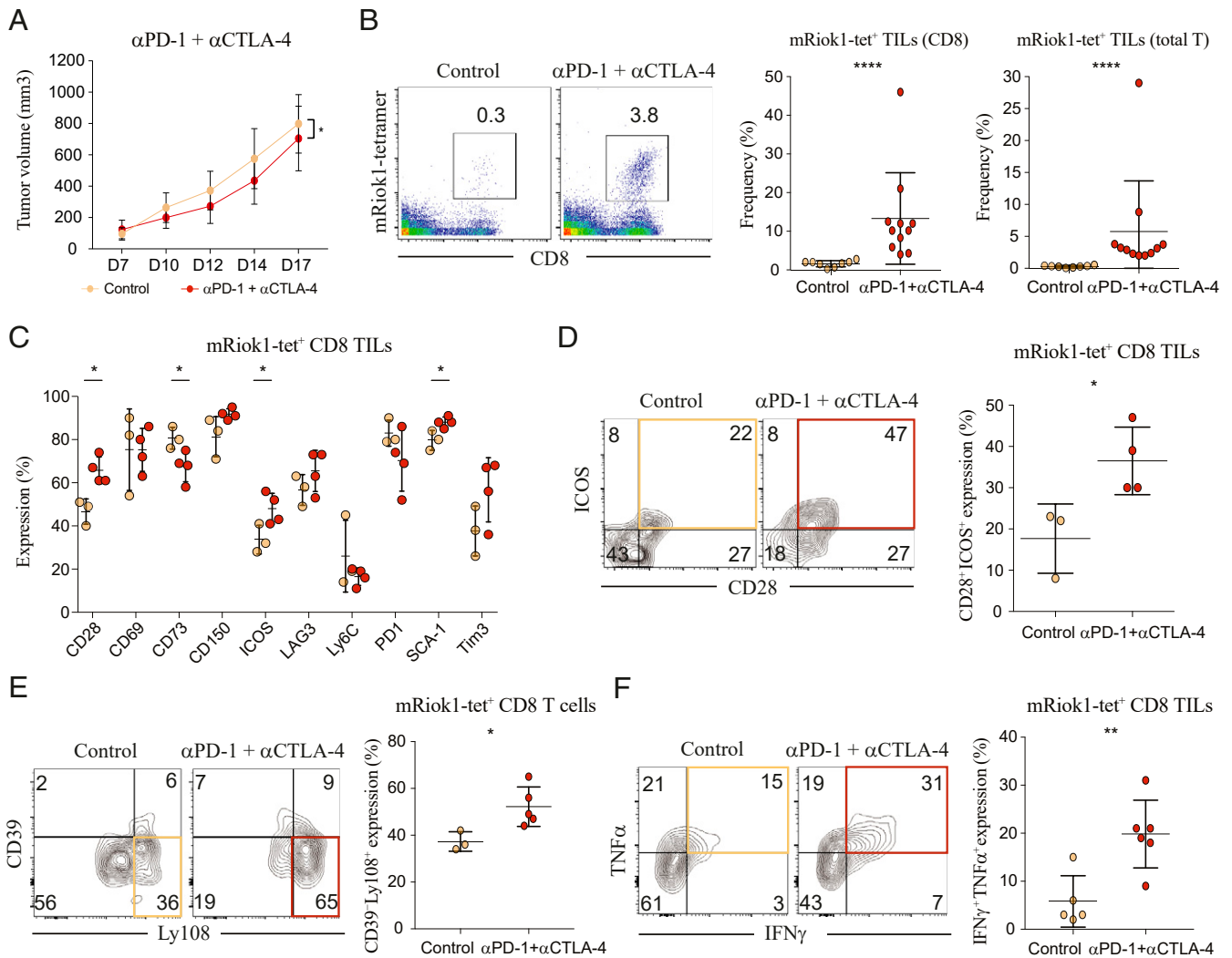


Fig. 4. Combining anti-PD-1 and anti-CTLA-4 blockades slightly improves tumor response with functional stem-like neoantigen-specific T cells. (A) LLC tumor growth measured as tumor volume in mm³ throughout treatment in anti-PD-1 + anti-CTLA-4 or control group. $n = 12$ to 25, data from four independent experiments, two-way ANOVA. (B) Representative mRiok1-tetramer staining among total TILs, gated against CD8, in anti-PD-1 + anti-CTLA-4-treated or control mice (Left). Frequencies of mRiok1-tet⁺ TILs among total CD8⁺ TILs and total TILs (Right). $n = 8$ to 11, means with SD, data from three independent experiments. Mann-Whitney unpaired *t* test. (C) Expression of selected markers on mRiok1-tet⁺CD8⁺ TILs from anti-PD-1 + anti-CTLA-4-treated or control group, $n = 3$ to 4, means with SD, Mann-Whitney unpaired *t* test. (D) Representative staining of ICOS and CD28 expression on mRiok1-tet⁺CD8⁺ TILs, from anti-PD-1 + anti-CTLA-4-treated or control group (Left). Frequencies of CD28⁺ICOS⁺ cells on mRiok1-tet⁺CD8⁺ TILs (Right). $n = 3$ to 4, means with SD, Mann-Whitney unpaired *t* test. (E) Representative staining of CD39 and Ly108 expression on mRiok1-tet⁺CD8⁺ T cells from draining lymph nodes of anti-PD-1 + anti-CTLA-4-treated or control group (Left). Frequencies of CD39⁺Ly108⁺ mRiok1-tet⁺CD8⁺ T cells (Right). $n = 3$ to 5, means with SD, Mann-Whitney unpaired *t* test. (F) Representative staining of TNF- α and IFN- γ production on mRiok1-tet⁺CD8⁺ TILs upon PMA/Ionomycin stimulation in anti-PD-1 + anti-CTLA-4-treated or control group (Left). Frequencies of TNF- α ⁺IFN- γ ⁺ cells on mRiok1-tet⁺CD8⁺ TILs (Right). $n = 5$ to 6, data from two independent experiments, means with SD, Mann-Whitney unpaired *t* test.

neoantigen-specific CD8⁺ TILs treated with anti-PD-1 + anti-CTLA-4, we analyzed the draining lymph nodes by flow cytometry and assessed the expression of both CD39 (exhaustion marker) and Ly108 [also known as SLAMF6, stem-like T cell marker (25, 27, 29, 49)]. We observed a higher frequency of CD39⁺Ly108⁺ mRiok1-specific CD8⁺ T cells, indicating accumulation of peripheral neoantigen-specific CD8⁺ T cells with stem-like characteristics (Fig. 4E and SI Appendix, Fig. S3A). Finally, we showed that neoantigen-specific CD8⁺ TILs after combination therapy were capable of producing more IFN- γ and TNF- α compared to the control group (Fig. 4F and SI Appendix, Fig. S3B).

Taken together, these results showed that neoantigen-specific T cells acquired a stem-like profile and polyfunctionality properties after anti-PD-1 and anti-CTLA-4 combined therapy. Nonetheless, LLC tumors remained resistant to the treatment.

Neoantigen-Specific T Cells Expand in Tumors Resistant to Neoantigen Vaccination. With the advent of neoantigen-associated therapies for cancer treatment and especially neoantigen vaccines (14–16), we investigated whether neoantigen immunization alone or in combination with immunotherapy would improve antitumor response. We first assessed the effectiveness of vaccination by immunizing a wild-type mouse (i.e., LLC-tumor free) with the mRiok1 peptide. A week after neoantigen peptide vaccination, we detected mRiok1-specific CD8⁺ T cells in the blood, spleen, and lymph nodes of vaccinated mice but not in the control mice, confirming the validity of our vaccination approach in inducing a neoantigen-specific CD8⁺ T cell response (Fig. 5A). Next, we evaluated the frequencies of mRiok1-specific CD8⁺ TILs following neoantigen vaccine and observed an expansion of these cells compared to the control group (Fig. 5B). However, we found no difference in tumor growth

between both groups (Fig. 5C). Similarly, in both combinations of neoantigen peptide vaccine with monotherapy treatment (anti-PD-1 or anti-CTLA-4) or dual treatment (anti-PD-1 + anti-CTLA-4) following tumor inoculation, we did not observe a better antitumor response compared with the control group (Fig. 5D and E). Interestingly, no synergistic effect was observed between neoantigen vaccine and immune checkpoint blockade (ICB) treatment in enriching the tumor neoantigen-specific T cell pool. mRiok1-tet⁺ CD8⁺ T cells from the tumors of all vaccinated mice (alone or in combination with ICB treatment) showed an exhausted phenotype (CD39⁺PD-1⁺) and are dysfunctional, and fewer cells in periphery are found to be stem-like (CD39⁻Ly108⁺) compared to the

untreated group (SI Appendix, Fig. S4). Altogether, these data showed that while neoantigen vaccination with mRiok1 elicited to an endogenous immune recognition, it did not help improve response to immunotherapy in LLC tumors.

Discussion

For the past 5 y, preclinical models have showed the feasibility to predict, identify, and develop vaccines using neoantigen(s). In human tumors, neoantigen-specific T cells were identified and characterized (50, 51). Case reports provided evidence that these cells (CD8 and CD4) can be harnessed to mediate tumor regression (52, 53), and phase I clinical trials demonstrated that

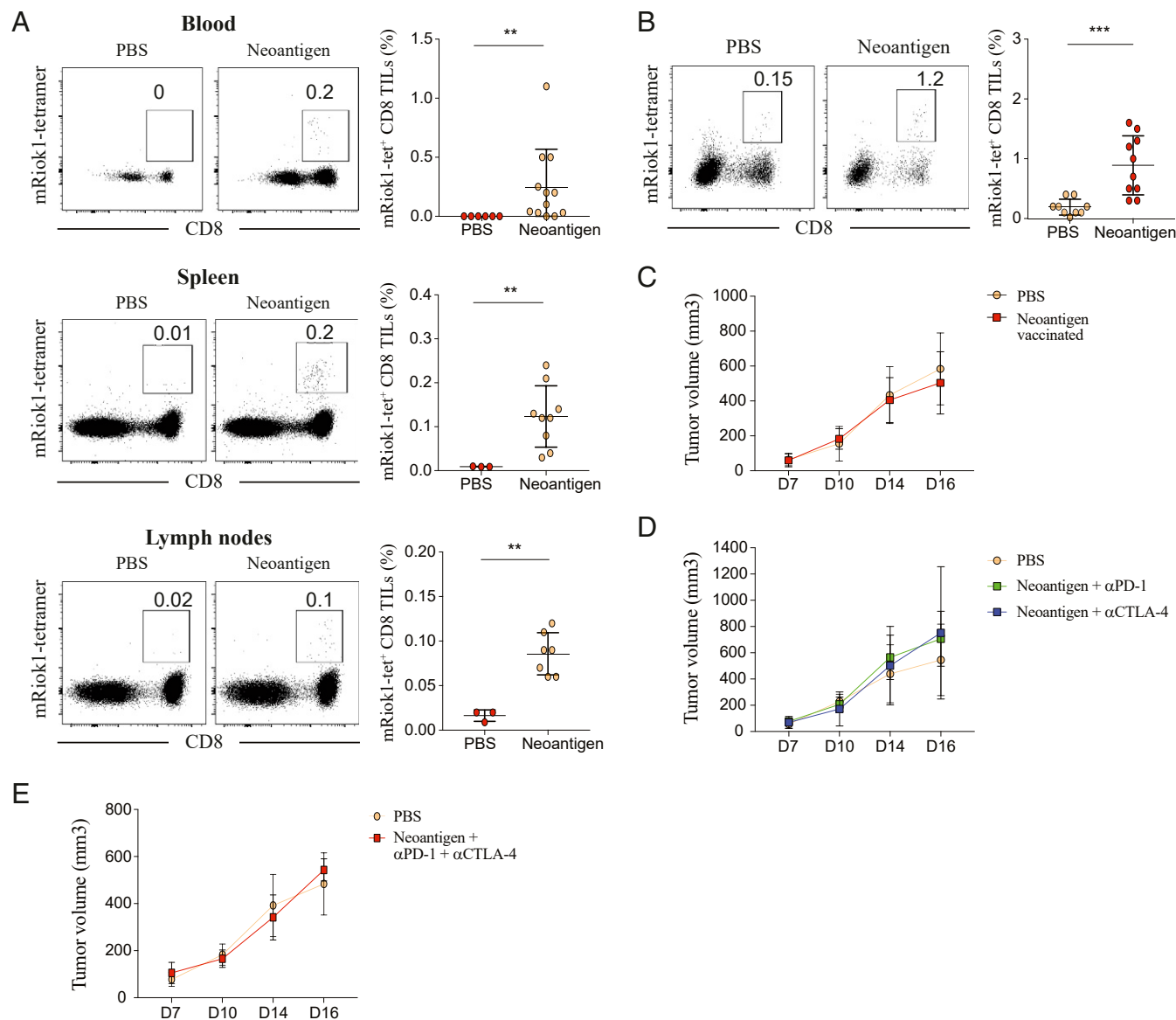


Fig. 5. Neoantigen-specific T cells expand in tumors resistant to neoantigen vaccination. (A) Representative mRiok1-tetramer staining among total T cells, gated against CD8, from blood, spleen, and lymph nodes of wild-type B6 mice vaccinated with neoantigen mRiok1 or PBS (Left). Frequencies of mRiok1-tet⁺ TILs among total TILs (Right). *n* = 3 to 12, data from two to three independent experiments, means with SD, Mann-Whitney unpaired *t* test. (B) Representative mRiok1-tetramer staining among total TILs in the tumors, gated against CD8, from mice vaccinated with neoantigen mRiok1 or control PBS (Left). Frequencies of mRiok1-tet⁺ TILs among total TILs (Right). *n* = 9 to 10, data from three independent experiments, means with SD, Mann-Whitney unpaired *t* test. (C) LLC tumor growth measured as tumor volume in mm³ from mice vaccinated with neoantigen mRiok1 or control PBS, *n* = 13 to 14, data from four independent experiments, means with SD. (D) LLC tumor growth measured as tumor volume in mm³ from mice vaccinated with neoantigen mRiok1 and treated with anti-PD-1 or anti-CTLA-4 or control PBS, *n* = 5 to 7, data from two independent experiments, means with SD. (E) LLC tumor growth measured as tumor volume in mm³ from mice vaccinated with neoantigen mRiok1 and treated with anti-PD-1 + anti-CTLA-4 or control PBS, *n* = 3, means with SD.

neoantigen vaccines are immunogenic (14, 16). While neoantigen identification has become the “gold rush” in the era of immunotherapy, neoantigen-based therapy is not a magic bullet to cure cancer. For instance, tumor cells can escape neoantigen-specific T cells by losing MHC class I allele–presenting neoantigen (53). Neoantigen-specific T cells can also become exhausted and require ICB therapy to restore their functions (e.g., anti-PD-1).

In this work, we showed that in the context of LLC tumor, neoantigen-specific CD8⁺ T cells are expanded after ICB monotherapies but accumulate in the tumors as exhausted cells and fail to elicit a potent antitumor response. When treated with dual therapy (anti-PD-1 and anti-CTLA-4), LLC tumors showed a slightly slower growth with some of the neoantigen-specific CD8⁺ T cells acquiring characteristics of stem-like T cells (expression of CD28, ICOS, and Ly108). This is in line with recent studies showing correlation between stem-like tumor-reactive T cells and clinical benefits, by opposition to terminally differentiated neoantigen-specific T cells that lead to a poor clinical response (30, 54). It is known that ICB dual and monotherapies have distinct cellular and molecular mechanisms. Notably, tumor-infiltrating T cells in dual-therapy–treated mice present an enhancement of T cell effector genes and cytokine response in the tumors (21, 55), and recent studies have shown an expansion of activated effector CD8⁺ T cells as well (46, 47). In our study, we showed that mRiok1-tet⁺ CD8⁺ T cells from combined therapy acquired a higher proportion of stem-like cells and a more functional profile and yet displayed an insufficient response to the treatment. Whether these data applicable to one neoantigen in a particular model is representative or only specific to this antigen remains to be explored. Furthermore, understanding what could be still missing for these cells would be crucial, and one unexplored aspect of our study is the impact of the tumor microenvironment, including the role of other immune cells (33, 56, 57). It would be interesting to investigate, for instance, the role of neoantigen-specific CD4⁺ T cells in LLC, as it was described to be essential for antitumor response in MCA sarcoma (23). One could also establish mutated cell lines to express mRiok1 de novo and assess neoantigen vaccination in an ICB-responsive model. On the other hand, understanding how combination treatment induces more stem-like neoantigen-specific CD8⁺ TILs is essential, as it would help improve current therapies by expanding stem-like T cells or restoring the functionality of exhausted cells. Recent works support the differentiation of stem-like into terminally exhausted T cells, favoring the maintenance of stem-like cells at their state instead of a potential reversion of the terminally exhausted T cells. Further single-cell transcriptomic and spatial analyses on mRiok1-tet⁺CD8⁺ TILs could help decipher the mechanistic pathways underlying the antitumor response and unravel the heterogeneity and dynamics within these cells.

ICB therapy combined with neoantigen vaccine has emerged as a new approach to boost antitumor response. The rationale using cancer vaccine in combination with ICB is to induce a long-term control of the disease by inducing a strong neoantigen response (58), and preclinical studies have showed tumor eradication using this strategy (59, 60). However, our results did not show improvement in antitumor response. One possible explanation could be the fact that we vaccinated with only a single MHC-I–restricted neoantigen, thus administering vaccine with epitope(s) targeting CD4 T cells as well could lead to a better efficiency in antitumor response (23). Another possibility could be related to the vaccine modalities used in this study that are not fully representative of the clinical settings (prophylactic context) and might not have employed the optimal route and adjuvant (33, 61).

Thus far, mouse models that have been used to study cancer neoantigens consist of immunotherapy responder models with a

high tumor mutation burden (20, 21). It is commonly established that neoantigen load, tumor mutation burden, and patient survival/response to immunotherapy are correlated (10, 18, 62). However, our data reconsider this consensus, as we observed a clear neoantigen-specific T cell expansion in a nonresponder model. Several works have recently pointed this discrepancy as well, in different types of cancers with or without immunotherapy treatment (51, 63, 64). This dissociation could be explained by neoantigen clonality as previously reported (50, 65). In that event, resistance would be conferred by selection of subclonal mutations with low immunogenicity (50, 66, 67). Another possibility could be copy number loss of tumor suppression genes that lead to elimination of neoantigen-expressing tumor clones during treatment (68). However, next-generation sequencing of the mRiok1 locus reveals that mutant allele frequencies of mRiok1 are stable in vivo regardless of the treatment regimen (*SI Appendix, Fig. S5A*). This suggests that even though there is a significant expansion of mRiok1-specific CD8⁺ T cells following ICB treatment, there is no strong selection against cancer cells harboring the neoantigen. In addition, we showed maintenance of MHC-I and -II expression on tumors treated with ICB, excluding the possibility of target antigen loss (*SI Appendix, Fig. S5B*).

Overall, our work provides a model to study mouse tumor neoantigens and revisits the role of tumor-specific CD8⁺ T cells in response to immunotherapy. We reinforce the importance for tumor-specific T cells to sustain stem-like and effector properties and highlight that neoantigen-specific CD8⁺ T cells alone can be insufficient to mediate an effective antitumor response in this model. Since LLC is a model with a relatively low tumor mutation load, our work could be translated into immunologically cold epithelial human tumors with low to moderate response to ICB, as well as cancer types with an excessively low rate of ex vivo neoantigen-specific CD8⁺ T cells being detected from in silico prediction (51). We believe this study will lead to important considerations in improving current therapeutic approaches and developing new anticancer strategies.

Materials and Methods

Neoantigen Prediction. Whole exome and RNA sequencing, mutation calling, and neoantigen prediction were performed as previously described (69). Briefly, somatic single nucleotide variants (SNVs) were identified from exome sequencing data. Variants were annotated, and SNVs were filtered to identify nonsynonymous, exonic variants. MHC-I binding affinity of LLC SNVs were predicted for H2-Db and H2-Kb haplotypes. Predicted MHC-I binders were selected based on their relative ranking in NetMHCpan 2.8, where the top 0.5% of ranked peptides were considered strong binders, top 2% ranked peptides weak binders, and those ranked >2% nonbinders, giving us 2,700 candidates. The expression of predicted strong and weak binders was confirmed with RNA sequencing data and candidates with >1 fragments per kilobase per million, the mutant allele expressed, and a predicted MHC-1 binding affinity of <500 nm was further selected resulting in 209 peptides.

Mice. All experiments were performed with C57BL/6 female mice aged from 5 to 12 wk and purchased from Jackson Laboratory. All experiments were conducted at Fred Hutchinson Cancer Research Center according to approved Institutional Animal Care and Use Committee protocols.

LLC Tumor Inoculation and Antibody Treatment. LLC tumor cells were obtained from B.W.R. laboratory and cultured following American Type Culture Collection guidelines. Briefly, cells were thawed from frozen stocks and expanded using Dulbecco’s modified eagle medium–based growth medium containing 10% heat-inactivated fetal bovine serum. When tumor cells reached 70 to 80% confluency, they were trypsinized, washed with phosphate-buffered saline (PBS), filtered, and resuspended in 10 M/mL. All B6 mice were injected with 1 M of cells (100ul) subcutaneously on the right hind flank, and tumor growth was monitored every 2 to 3 d. Tumor width and length were measured using calipers, and mice were euthanized if tumor volume exceeded 2,000 mm³ or became inflamed/ulcerated. For antibody treatment, mice were treated intraperitoneally with 200 μg of either anti-PD-1 (murine IgG2a, clone RMP1-14) and/or anti-CTLA-4 (murine IgG2b, clone 9D9) or their respective

isotype control (IgG2a, clone 2A3, IgG2b, clone MPC-11) on day 7, 10, and 14 post-tumor inoculation. All antibodies were purchased from BioXcell.

Neoantigen Vaccination. Mice were prophylactically vaccinated subcutaneously with 100 μ g of mRiok1 peptide in 100 μ L PBS in combination with 1:1 volume of Complete Freund's Adjuvant (InvivoGen) (day -12). Blood was collected on day 7 and fluorescence-activated cell sorting (FACS) stained to confirm the presence of mRiok1-tet⁺ CD8 T cells (day -5). Mice were boosted with another shot of neoantigen vaccine, and tumor cells were injected 5 d after (day 0). When applicable, anti-PD-1 and/or anti-CTLA-4 treatment was given as described in the *Antibody Treatment* section. As controls, mice were immunized with either PBS or the mRiok1 peptide alone.

Antibodies and SAV. Purified antibodies lacking carrier proteins were purchased according to the list in Table S2. Antibody conjugation was performed according to the protocol provided by Fluidigm. Streptavidin was labeled as previously described (35).

MHC Monomer Production and Multiplex Tetramer Preparation. H2K^b and H2D^b pMHC complexes were synthesized in house as previously described (35). Specific pMHC monomers were then generated by ultraviolet (UV) irradiation using the peptides of interest as described previously (22, 51). Briefly, 5 μ L of each of the 209 peptides at 1 mM was added to 100 μ L corresponding H2 monomer (Kb or Db) at 100 μ g/mL in a 96-well plate. A total of 11 control peptides (LCMV, Flu, and OVA) were also included (Table S1). The three plates were then placed in a UV crosslinker (365 nm) for 10 min and kept in the refrigerator at least overnight before tetramerization.

For multiplex MHC-tetramer staining, each tetramer was labeled with a combination of three metal-labeled SAV. Using 12 different metal-labeled SAV, 220 possible combinations (12 choose 3) were generated. Each specific combination was associated with a different peptide. Each metal-labeled streptavidin (50 μ g/mL) was mixed for each combination using an automated pipetting device (TECAN). For tetramerization, each peptide-MHC complex-metal-labeled-streptavidin combination (50 μ g/mL) was added in three steps (3 \times 20 μ L) according to the coding scheme. Then, tetramerized pMHC complexes were incubated with free biotin for 10 min (10 μ M, Sigma). All different tetramers were combined and concentrated using a 50-kDa Amicon filter (Millipore) to a final volume of 500 μ L. Then, 500 μ L PBS, 1% bovine serum albumin, and 0.02% sodium azide was added. Before staining, the tetramer mixture was filtered using a 0.1- μ m filter (Millipore).

Tissue Collection, Cell Isolation, and Preparation. At 14- to 16-d post-tumor inoculation (or before when applicable), mice were euthanized and tumors and different peripheral organs (draining lymph nodes (LNs), lungs, spleen, non-draining LNs, and blood) were collected. Tumors and lungs were mechanically dissociated into small pieces and digested at 37 $^{\circ}$ C for 1 h in Roswell Park Memorial Institute Medium (RPMI) + collagenase IV (1 mg/mL) + DNase (10 μ g/mL) (both from Sigma). For spleen and blood, red blood cells were removed using 1 \times red blood cell lysis buffer (ThermoFisher). Single-cell suspensions were then filtered through a 70- μ m strainer and washed using RPMI. For tumor samples, cells were then enriched for T cells using negative selection (mouse pan T cell isolation kit II, Miltenyi) and selected for CD45-positive cells (mouse CD45 microbeads, Miltenyi) before proceeding to flow cytometry or CyTOF staining.

PMA/Ionomycin Stimulation and Flow Cytometry Intranuclear Staining. Following cell isolation and preparation, samples were stained for FACS using mRiok1-tetramer (1 h at room temperature) and surface antibodies (20 min each at 4 $^{\circ}$ C) in Table S2. For intranuclear staining, cells were fixed and permeabilized using Foxp3 transcription factor staining buffer set (eBioscience) and incubated with intracellular antibodies for 30 min at 4 $^{\circ}$ C. Samples were run on BD FACSCelesta and analyzed using FlowJo. For evaluation of cytokine production,

samples were stimulated before staining with PMA at 50 ng/mL and Ionomycin at 1 μ g/mL (Sigma) along with Brefeldin A at 1 \times (eBioscience) for 4 h. mRiok1-tetramer and subsequent antibodies stainings were carried on after a wash in FACS buffer. For MHC-I and MHC-II expression, tumors from different treatment conditions were surface stained at D16 with antibodies in Table S2 and 7-AAD (Biolegend) following manufacturer's instructions.

CytoF Staining. Cells were stained with 5 μ M cisplatin (viability marker) in PBS for 5 min at 4 $^{\circ}$ C as previously described (70, 71), followed by the tetramer mixture for 1 h at room temperature and the antibody mixture for 15 min at 4 $^{\circ}$ C (Table S2). Cells were then fixed in 2% paraformaldehyde overnight. The following day, cells were washed using PBS, barcoded using a single combination of two in-house bromoacetamidobenzyl-ethylenediamine tetraacetic acid (Dojindo)-linked metal barcodes diluted in PBS (Pd-102, Pd-104, Pd106, Pd108, or Pd-110) for each sample, for 30 min at 4 $^{\circ}$ C. Cells were washed again and stained with DNA (Cell-ID intercalator-Ir, Fluidigm) for 10 min at room temperature. After three more washes with dH₂O, samples were combined and acquired on CyTOF as previously described (10, 72).

UMAP Analysis. After mass cytometry (CyTOF) acquisition, any zero values were randomized using a uniform distribution of values between 0 and -1 using R. The signal of each parameter was normalized based on EQ beads (Fluidigm) as described previously (73). Each sample was debarcoded using manual gating on FlowJo. Exported samples or cells of interest were then exported and used for UMAP analysis similar to that previously described using customized R scripts based on the "flowCore" and "uwot" R packages (37). In R, all data were transformed using the logicleTransform function (flowCore package) using the following parameters: $w = 0.25$, $t = 16,409$, $m = 4.5$, and $a = 0$ to roughly match scaling historically used in FlowJo. For heatmaps, median intensity corresponds to a logical data scale using formula previously described (74). The colors in the heat map represent the measured means intensity value of a given marker in a given sample. A seven-color scale is used with black-blue indicating low expression values, green-yellow indicating intermediately expressed markers, and orange-red representing highly expressed markers.

Genomic DNA Isolation and Targeted Sequencing. Genomic DNA was isolated from 10 mg tumor tissue using the Qiagen DNeasy Blood and Tissue Kit (Cat No. 69504) per the manufacturer's instructions. A total of 50 ng genomic DNA was used as input for PCR amplification of the *RIOK1* locus, using primers containing Illumina barcodes compatible with next generation sequencing platforms (FWD: AACTCTTTCCCTACACGACGCTCTCCGATCTcccttttcattccagccagcc, REV: GACTGGAGTTCAGACGTGTGCTCTCCGATCTcaca-gtacag-cgggactgc). The resulting amplicon was purified using a 1 \times AMPureXP Bead clean up per manufacturer's instructions (Beckman Coulter Life Sciences Part No. A63881). The purified product was submitted to GENEWIZ for AmpliconEZ sequencing. Reads were mapped to the predicted amplicon and mutation frequencies were quantified using the CRISPResso computational pipeline (75).

Data Availability. All study data are included in the article and/or supporting information.

ACKNOWLEDGMENTS. We thank all members of the E.N. laboratory, Fred Hutchinson Cancer Research Center, Seattle. We thank Mark Headley and Maximilien Evrard for their feedback and insights. We thank Chen Xiaoyang, the members from the flow and immunogenomic platforms, as well as the Comparative Medicine team of the Fred Hutchinson Cancer Research Center. R.K.B. is a Scholar of The Leukemia & Lymphoma Society (1344-18). This study was funded by The Andy Hill Endowment Distinguished Researcher Cancer Research Endowment fund to E.W.N.

- D. M. Pardoll, The blockade of immune checkpoints in cancer immunotherapy. *Nat. Rev. Cancer* **12**, 252–264 (2012).
- S. C. Wei, C. R. Duffy, J. P. Allison, Fundamental mechanisms of immune checkpoint blockade therapy. *Cancer Discov.* **8**, 1069–1086 (2018).
- P. Sharma, S. Hu-Lieskovan, J. A. Wargo, A. Ribas, Primary, adaptive, and acquired resistance to cancer immunotherapy. *Cell* **168**, 707–723 (2017).
- A. Kalbasi, A. Ribas, Tumour-intrinsic resistance to immune checkpoint blockade. *Nat. Rev. Immunol.* **20**, 25–39 (2020).
- M. Peng *et al.*, Neoantigen vaccine: An emerging tumor immunotherapy. *Mol. Cancer* **18**, 128 (2019).
- Y. C. Lu, P. F. Robbins, Cancer immunotherapy targeting neoantigens. *Semin. Immunol.* **28**, 22–27 (2016).
- T. N. Schumacher, R. D. Schreiber, Neoantigens in cancer immunotherapy. *Science* **348**, 69–74 (2015).
- T. N. Schumacher, W. Scheper, P. Kvistborg, Cancer Neoantigens. *Annu. Rev. Immunol.* **37**, 173–200 (2019).
- N. van Rooij *et al.*, Tumor exome analysis reveals neoantigen-specific T-cell reactivity in an ipilimumab-responsive melanoma. *J. Clin. Oncol.* **31**, e439–e442 (2013).
- N. A. Rizvi *et al.*, Cancer immunology. Mutational landscape determines sensitivity to PD-1 blockade in non-small cell lung cancer. *Science* **348**, 124–128 (2015).
- S. Stevanović *et al.*, Landscape of immunogenic tumor antigens in successful immunotherapy of virally induced epithelial cancer. *Science* **356**, 200–205 (2017).
- D. T. Le *et al.*, Mismatch repair deficiency predicts response of solid tumors to PD-1 blockade. *Science* **357**, 409–413 (2017).

13. M. M. Gubin, M. N. Artyomov, E. R. Mardis, R. D. Schreiber, Tumor neoantigens: Building a framework for personalized cancer immunotherapy. *J. Clin. Invest.* **125**, 3413–3421 (2015).
14. P. A. Ott *et al.*, An immunogenic personal neoantigen vaccine for patients with melanoma. *Nature* **547**, 217–221 (2017).
15. D. B. Keskin *et al.*, Neoantigen vaccine generates intratumoral T cell responses in phase Ib glioblastoma trial. *Nature* **565**, 234–239 (2019).
16. U. Sahin *et al.*, Personalized RNA mutanome vaccines mobilize poly-specific therapeutic immunity against cancer. *Nature* **547**, 222–226 (2017).
17. A. Garcia-Garjito, C. A. Fajardo, A. Gros, Determinants for neoantigen identification. *Front. Immunol.* **10**, 1392 (2019).
18. E. M. Van Allen *et al.*, Genomic correlates of response to CTLA-4 blockade in metastatic melanoma. *Science* **350**, 207–211 (2015).
19. K. Kim *et al.*, Predicting clinical benefit of immunotherapy by antigenic or functional mutations affecting tumour immunogenicity. *Nat. Commun.* **11**, 951 (2020).
20. M. Yadav *et al.*, Predicting immunogenic tumour mutations by combining mass spectrometry and exome sequencing. *Nature* **515**, 572–576 (2014).
21. M. M. Gubin *et al.*, Checkpoint blockade cancer immunotherapy targets tumour-specific mutant antigens. *Nature* **515**, 577–581 (2014).
22. M. Fehlings *et al.*, Checkpoint blockade immunotherapy reshapes the high-dimensional phenotypic heterogeneity of murine intratumoural neoantigen-specific CD8⁺ T cells. *Nat. Commun.* **8**, 562 (2017).
23. E. Alspach *et al.*, MHC-II neoantigens shape tumour immunity and response to immunotherapy. *Nature* **574**, 696–701 (2019).
24. M. M. Gubin *et al.*, High-dimensional analysis delineates myeloid and lymphoid compartment remodeling during successful immune-checkpoint cancer therapy. *Cell* **175**, 1014–1030.e19 (2018).
25. I. Siddiqui *et al.*, Intratumoral Tcf1⁺PD-1⁺CD8⁺ T cells with stem-like properties promote tumor control in response to vaccination and checkpoint blockade immunotherapy. *Immunity* **50**, 195–211.e10 (2019).
26. S. Kurtulus *et al.*, Checkpoint blockade immunotherapy induces dynamic changes in PD-1⁺CD8⁺ tumor-infiltrating T cells. *Immunity* **50**, 181–194.e6 (2019).
27. A. Kallies, D. Zehn, D. T. Utzschneider, Precursor exhausted T cells: Key to successful immunotherapy? *Nat. Rev. Immunol.* **20**, 128–136 (2020).
28. S. J. Im *et al.*, Defining CD8⁺ T cells that provide the proliferative burst after PD-1 therapy. *Nature* **537**, 417–421 (2016).
29. D. T. Utzschneider *et al.*, T cell factor 1-expressing memory-like CD8(+) T cells sustain the immune response to chronic viral infections. *Immunity* **45**, 415–427 (2016).
30. B. C. Miller *et al.*, Subsets of exhausted CD8⁺ T cells differentially mediate tumor control and respond to checkpoint blockade. *Nat. Immunol.* **20**, 326–336 (2019).
31. W. J. Lesterhuis *et al.*, Synergistic effect of CTLA-4 blockade and cancer chemotherapy in the induction of anti-tumor immunity. *PLoS One* **8**, e61895 (2013).
32. F. Bertrand *et al.*, TNF α blockade overcomes resistance to anti-PD-1 in experimental melanoma. *Nat. Commun.* **8**, 2256 (2017).
33. H. Y. Li *et al.*, The tumor microenvironment regulates sensitivity of murine lung tumors to PD-1/PD-L1 antibody blockade. *Cancer Immunol. Res.* **5**, 767–777 (2017).
34. M. Sharma *et al.*, Bempedalsleukin selectively depletes intratumoral Tregs and potentiates T cell-mediated cancer therapy. *Nat. Commun.* **11**, 661 (2020).
35. E. W. Newell *et al.*, Combinatorial tetramer staining and mass cytometry analysis facilitate T-cell epitope mapping and characterization. *Nat. Biotechnol.* **31**, 623–629 (2013).
36. E. W. Newell, L. O. Klein, W. Yu, M. M. Davis, Simultaneous detection of many T-cell specificities using combinatorial tetramer staining. *Nat. Methods* **6**, 497–499 (2009).
37. E. Becht *et al.*, Dimensionality reduction for visualizing single-cell data using UMAP. *Nat. Biotechnol.* **10.1038/nbt.4314** (2018).
38. J. A. Seidel, A. Otsuka, K. Kabashima, Anti-PD-1 and Anti-CTLA-4 therapies in cancer: Mechanisms of action, efficacy, and limitations. *Front. Oncol.* **8**, 86 (2018).
39. V. A. Pedicord, W. Montalvo, I. M. Leiner, J. P. Allison, Single dose of anti-CTLA-4 enhances CD8⁺ T-cell memory formation, function, and maintenance. *Proc. Natl. Acad. Sci. U.S.A.* **108**, 266–271 (2011).
40. I. Tóth *et al.*, Decreased frequency of CD73⁺CD8⁺ T cells of HIV-infected patients correlates with immune activation and T cell exhaustion. *J. Leukoc. Biol.* **94**, 551–561 (2013).
41. F. P. Canale *et al.*, CD39 expression defines cell exhaustion in tumor-infiltrating CD8⁺ T cells-response. *Cancer Res.* **78**, 5175 (2018).
42. Y. Kong *et al.*, Downregulation of CD73 associates with T cell exhaustion in AML patients. *J. Hematol. Oncol.* **12**, 40 (2019).
43. C. Blanc *et al.*, Targeting resident memory T cells for cancer immunotherapy. *Front. Immunol.* **9**, 1722 (2018).
44. S. Corgnac, M. Boutet, M. Kfoury, C. Naltet, F. Mami-Chouaib, The emerging role of CD8⁺ tissue resident memory T (T_{RM}) cells in antitumor immunity: A unique functional contribution of the CD103 integrin. *Front. Immunol.* **9**, 1904 (2018).
45. J. Edwards *et al.*, CD103⁺ tumor-resident CD8⁺ T cells are associated with improved survival in immunotherapy-naïve melanoma patients and expand significantly during anti-PD-1 treatment. *Clin. Cancer Res.* **24**, 3036–3045 (2018).
46. S. C. Wei *et al.*, Combination anti-CTLA-4 plus anti-PD-1 checkpoint blockade utilizes cellular mechanisms partially distinct from monotherapies. *Proc. Natl. Acad. Sci. U.S.A.* **116**, 22699–22709 (2019).
47. T. N. Gide *et al.*, Distinct immune cell populations define response to anti-PD-1 monotherapy and anti-PD-1/Anti-CTLA-4 combined therapy. *Cancer Cell* **35**, 238–255.e6 (2019).
48. L. Gattinoni *et al.*, Wnt signaling arrests effector T cell differentiation and generates CD8⁺ memory stem cells. *Nat. Med.* **15**, 808–813 (2009).
49. Y. A. Leong *et al.*, CXCR5(+) follicular cytotoxic T cells control viral infection in B cell follicles. *Nat. Immunol.* **17**, 1187–1196 (2016).
50. N. McGranahan *et al.*, Clonal neoantigens elicit T cell immunoreactivity and sensitivity to immune checkpoint blockade. *Science* **351**, 1463–1469 (2016).
51. Y. Simoni *et al.*, Bystander CD8⁺ T cells are abundant and phenotypically distinct in human tumour infiltrates. *Nature* **557**, 575–579 (2018).
52. E. Tran *et al.*, Cancer immunotherapy based on mutation-specific CD4⁺ T cells in a patient with epithelial cancer. *Science* **344**, 641–645 (2014).
53. E. Tran *et al.*, T-cell transfer therapy targeting mutant KRAS in cancer. *N. Engl. J. Med.* **375**, 2255–2262 (2016).
54. S. Krishna *et al.*, Stem-like CD8 T cells mediate response of adoptive cell immunotherapy against human cancer. *Science* **370**, 1328–1334 (2020).
55. M. A. Curran, W. Montalvo, H. Yagita, J. P. Allison, PD-1 and CTLA-4 combination blockade expands infiltrating T cells and reduces regulatory T and myeloid cells within B16 melanoma tumors. *Proc. Natl. Acad. Sci. U.S.A.* **107**, 4275–4280 (2010).
56. C. S. Jansen *et al.*, An intra-tumoral niche maintains and differentiates stem-like CD8 T cells. *Nature* **576**, 465–470 (2019).
57. B. L. Bullock *et al.*, Tumor-intrinsic response to IFN γ shapes the tumor microenvironment and anti-PD-1 response in NSCLC. *Life Sci. Alliance* **2**, e201900328 (2019).
58. V. Alcazar *et al.*, Neoepitopes-based vaccines: Challenges and perspectives. *Eur. J. Cancer* **108**, 55–60 (2019).
59. L. Karyampudi *et al.*, Accumulation of memory precursor CD8 T cells in regressing tumors following combination therapy with vaccine and anti-PD-1 antibody. *Cancer Res.* **74**, 2974–2985 (2014).
60. O. A. Ali, S. A. Lewin, G. Dranoff, D. J. Mooney, Vaccines combined with immune checkpoint antibodies promote cytotoxic T-cell activity and tumor eradication. *Cancer Immunol. Res.* **4**, 95–100 (2016).
61. U. Sahin *et al.*, An RNA vaccine drives immunity in checkpoint-inhibitor-treated melanoma. *Nature* **585**, 107–112 (2020).
62. V. Anagnostou *et al.*, Evolution of neoantigen landscape during immune checkpoint blockade in non-small cell lung cancer. *Cancer Discov.* **7**, 264–276 (2017).
63. A. E. Zamora *et al.*, Pediatric patients with acute lymphoblastic leukemia generate abundant and functional neoantigen-specific CD8⁺ T cell responses. *Sci. Transl. Med.* **11**, eaat8549 (2019).
64. A. Mauriello *et al.*, High somatic mutation and neoantigen burden do not correlate with decreased progression-free survival in HCC patients not undergoing immunotherapy. *Cancers (Basel)* **11**, E1824 (2019).
65. I. Milo *et al.*, The immune system profoundly restricts intratumor genetic heterogeneity. *Sci. Immunol.* **3**, eaat1435 (2018).
66. R. D. Schreiber, L. J. Old, M. J. Smyth, Cancer immunoediting: Integrating immunity's roles in cancer suppression and promotion. *Science* **331**, 1565–1570 (2011).
67. N. Riaz *et al.*, Tumor and microenvironment evolution during immunotherapy with nivolumab. *Cell* **171**, 934–949.e16 (2017).
68. K. Takeda *et al.*, IFN- γ is required for cytotoxic T cell-dependent cancer genome immunoediting. *Nat. Commun.* **8**, 14607 (2017).
69. S. Ma *et al.*, Pre-treatment tumor neo-antigen responses in draining lymph nodes are infrequent but predict checkpoint blockade therapy outcome. *Oncolimmunology* **9**, 1684714 (2019).
70. S. Li *et al.*, Human tumor-infiltrating MAIT cells display hallmarks of bacterial antigen recognition in colorectal cancer. *Cell Rep Med* **1**, 100039 (2020).
71. Y. Simoni *et al.*, Partial absence of PD-1 expression by tumor-infiltrating EBV-specific CD8⁺ T cells in EBV-driven lymphoepithelioma-like carcinoma. *Clin. Transl. Immunology* **9**, e1175 (2020).
72. B. Becher *et al.*, High-dimensional analysis of the murine myeloid cell system. *Nat. Immunol.* **15**, 1181–1189 (2014).
73. R. Finck *et al.*, Normalization of mass cytometry data with bead standards. *Cytometry A* **83**, 483–494 (2013).
74. W. A. Moore, D. R. Parks, Update for the logicle data scale including operational code implementations. *Cytometry A* **81**, 273–277 (2012).
75. K. Clement *et al.*, CRISPResso2 provides accurate and rapid genome editing sequence analysis. *Nat. Biotechnol.* **37**, 224–226 (2019).